A Review of Literature for the Flow Accelerated Corrosion of Mitred Bends

Muhammadu Masin Muhammadu[1], Jamaluddin Sheriff[2], Esah Hamzah[3]

[1]*Department of Mechanical Engineering, Federal University of Technology, Minna, Nigeria*
[2]*Department of Thermo-fluid Engineering, Universiti Teknologi Malaysia*
[3]*Department of Materials and Manufacturing Engineering, Universiti Teknologi Malaysia*

Abstract--**This paper present a state - of - the art review of literatures available for the flow accelerated corrosion of mitred bends. Compared with smooth bends, the volume of literature available for mitres is less extensive and its scope is not as wide. This review tabulates and characterises all publications to date in chronological order. The details of experimental specimens are highlighted with a view to these perhaps providing useful verification data for any future computational fluid modeling analysis for example. Flow accelerated corrosion in bends are discussed where relevant. Details of ultrasonic thickness measurement by ultrasonic testing, scanning electron microscopy, chemical analysis, stereomicroscopic test and x- ray diffraction (XRD) are revealed.**

Keywords-- **scanning electron microscopy, Magnification, impingement, Flow Accelerated Corrosion, Computational fluid dynamics, Microscopy**

I. INTRODUCTION

Flow Accelerated Corrosion (FAC) is distinct from erosion–corrosion and is primarily a corrosion process aided by chemical dissolution and mass transfer (1-7). In practice, there may be some contribution from the mechanical factors that lead to removal of corroded scallops on material surface to become loose and flow out with the high velocity process fluid. This might be further accelerating the overall FAC rate but would not become a factor for thinning by itself (i.e. without first the electrochemical dissolution leading to FAC and formation of loosely held scallops). The corrosion rate is first determined by the rate of transfer of ionic species between the surface and the fluid. If the corrosion reaction is rapid and the corrosion product has low solubility in bulk fluid, the corrosion rate is governed by the concentration gradient as shown in Equation (1), where CR is the corrosion rate, k is the mass transfer coefficient, C_W is the concentration of rate limiting species in the boundary layer at the metal wall, and C_B is the concentration of rate limiting species in the bulk fluid.

$$CR = k(C_w - C_B) \qquad (1)$$

Flow velocities associated with FAC increase this concentration gradient and thus increase the corrosion rate (1–9). No evidence of removal of the oxide film purely due to mechanical shear has been found on the FAC damaged surfaces of feed water piping (3). Erosion- corrosion is a form of mechanical degradation that involves corrosion as well as mechanical wear. This occurs on the surface of the material due to the action of numerous individual impacts of solid or liquid particles. Much higher flow velocities are associated with this kind of degradation. Laboratory tests have also shown that the fluid velocities required for mechanical removal of the oxide is higher than that required for dissolution of an oxide layer (3,7,9). Definite surface patterns are formed on components undergoing FAC which is a signature of FAC while no such signature is associated with erosion corrosion (8–11). Due to erosion corrosion grooves, gullies or rounded holes are formed while FAC affected surfaces have a wavy pattern [8–10]. This can occur in metals and alloys that are completely resistant to a particular environment at low flow velocities unlike FAC degradation (9).

Mitred bends are widely used in industry. In particular, applications include large-diameter pipe work or ducting in chemical processes, desalination plants, water supply and nuclear power stations, where the manufacture of smooth bends may be either impractical or uneconomical. In many cases, designers will prefer to utilise smooth pipe bends due to the lack of discontinuity, the relatively smaller stress concentration and the more favourable flow characteristics. However, in large-diameter applications or applications with restricted space or a tight budget, mitred bends still find application.

A detailed review and assessment of every document published on mitred bends is obviously not possible within the scope of this paper. The main aim of this review therefore is to draw attention to the information available in the open literature, to give the reader an indication of scope and to identify possible areas for further research, the challenge being to try and summarize this research in a useful manner to industry and academia today.

Many researchers have carried out both experimental and numerical modeling of the erosion-corrosion of mitre bends, elbows, tees and related geometries. Since the early 1990s, computational fluid dynamics (CFD) has been widely used for corrosion prediction in curved pipes and ducts, with various analytical, semi-empirical and empirical models have been developed. This provided a critical review of some of the corrosion models that had been developed (12). The first proposed analytical approach (13), and found 28 models that were specifically for solid particle–wall erosion. The authors reported that 33 parameters were used in these models, with an average of five parameters per model. These parameters influence the amount of material eroded from a target surface and the mechanism of erosion. The review revealed that each model equation was the result of a very specific and individual approach, hence it is clear that no single equation exists that can be used to predict wear from all known standard material or particle parameters, and that some reliance on experimental measurement will always be required to provide empirical constants necessary in the various erosion models. The following review is limited to models that have been used in CFD-based erosion modeling and which have received wide usage in applications to erosion in pipes and pipe fittings.

II. REVIEW OF LITERATURES ON MITRES

This paper presents an up-to-date and comprehensive list of all references relating to the flow accelerated erosion-corrosion of mitred pipe bends of all types. The general nature and content of these publications is presented in Table. A more extensive review of the literature, on all aspects of mitred bend behaviour is available in a supplement (20). This reference discusses the significant conclusions from each publication, which is obviously not possible in the present paper.

The (11) and (13)used an algebraic slip multiphase model, coupled with the (14 and 15) (1963a, 1963b) and (16) erosion models, to examine erosion due to slurry flow in straight pipes and bend. However, (17)also used an Eulerian–Lagrangian approach, coupled with a semi-empirical erosion equation, to predict erosion due to slurry flow in choke valves. The fluid phase modelling used the Reynolds averaged Navier-Stokes (RANS) equations, and either the standard k–ε model of Launder and (18) renormalized group (RNG) model of (19), in a commercial CFD code for turbulence closure.

The particle rebound angle and velocity were computed using the empirical restitution coefficient of (20). The authors also (21) erosion-corrosion equation by data fitting to the results of jet-type wear tests (22), and used the modified equation to predict erosion rate. The authors obtained good agreement with data for the flow field for both the simple and the complex geometries examined. However, they reported an under-prediction of the average erosion rate by 60% for the simple geometry, and an under-prediction of the complex geometry by a factor of 10–15. They attributed these under-predictions to the neglect of geometry changes in their models.

The (23) used an Eulerian–Lagrangian approach and semi-empirical erosion models to examine erosion in sudden pipe contractions (24, and Said, 2005; 25; 26, and Said, 2004; 27, 2008), and erosion in the tube end of the tube sheet of a shell-and-tube heat exchanger (28, Said, and 29, 2006; 27, Said, 28, 2006; 25, Said, and 29, 2005). Turbulence was modelled using the RNG k–∈ model in a commercial CFD code, and the authors employed the Wallace (2001) version of the Neilson and Gilchrist (1968) erosion equation to model erosion rates, and the erosion models developed at the University of Tulsa (30, 1994; 31., 2001; 32, 1993, 1996; 33, 1995) to compute the penetration rate (i.e. the depth of the eroded material/time period). The influence of the different parameters such as the inlet flow velocity, the particle diameter.

In 1994 (30) developed an empirical erosion model for AISI 1018 Steel. (32) (1993, 1996) extended this model for aluminium and used it to predict particle erosion resulting from cross-sections, and was subsequently referred to as E/CRC model. In 1996 (34) applied this model to investigate the effects of elbow radius of curvature on erosion rates in circulate pipe. Also, in 1995 (35) also developed mechanistic models for predicting corrosion in elbows based on the E/CRC model. Edwards, (31) in 1998 and 2001 used a commercial CFD code to model fluid solid flows and added routines to predict erosion on particle impact using the E/CRC model. And (36) in 2000; (37)in 1998 also modelled the erosion in oilfield control valves using a commercial CFD code, accounting for both deformation and cutting erosion. In 2000 (36) obtained a good agreement for the predicted wear rates and wear locations in mitre bends with the experimental gas–solid corrosion results of (38) in 1989.

(39) in 2004, (40 and 41) in 2006a, 2006b) added the stochastic rebound model of Grant and (42) in1975 and the E/CRC model (30) in 1994; (32) in 1993, 1996) to a commercially available CFD code, and investigated the relative erosion severity in elbows and plug tees found in oilfield geometries. Numerical simulations showed that particle rebound behaviour played an important role in determining the motion of the particles. The authors reported that the CFD-based erosion procedure was able to predict reasonably the erosion profile and satisfactorily showed the trend of erosion with respect to the carrier velocity.

In 2003 (43) performed their corrosion research on 900 elbows and bends of circular cross-section. The fluid phase was modeled using a simple modified mixing-length model. The predicted fluid axial velocity was validated against the experimental data of (44) in 994, with erosion-corrosion modelled using the E/CRC model (30), 1994; (32), 1993 and 1996. They compared their predicted penetration rates with the experimental data of (45) in1987, obtaining good qualitative agreement but poor quantitative agreement between the predictions and data. The poor agreement occurred because most of the data available were from erosion-corrosion experiments with high flow rates. The authors also found that erosion in long radius bends was reduced when the arrier phase was changed from liquid to gas. They further reported that the effect of the squeeze film, secondary flows and turbulent flow fluctuations may all play important roles in erosion prediction when the carrier fluid is a liquid.

In1991 (46) studied the local erosion in chokes by determining the local fluid velocity and particle impingement. Hence, in2000 (47) used a commercial CFD code coupled with an in-house particle tracker to predict fluid-particle flow in a full 180∘ bend. The authors implemented two erosion-corrosion models, namely those of Finnie (1960) and the (50) and Nesic model (48), 1984; (46) in 1991 to investigate erosion–corrosion problems in U-bends. However, no comparison was made with experimental data; hence, the validity of the model could not be ascertained. Hanson and (49) in 2000 attempted to account for the shape of wear scars in predicting the life of pneumatic conveyor bends undergoing erosive wear. However, these authors did not use the shape of the scar to alter the computational mesh used in the fluid phase calculations.

In 2009 (50) applied an Eulerian–Lagrangian approach with particle–particle interaction and a particle erosion model to simulate solid particle movement as well as the particle erosion characteristics of a solid–liquid two-phase flow in a choke of mitre bend. The authors used the standard k–∈ model to treat the turbulence, the discrete particle hard sphere model to accommodate inter-particle collisions, and the semi-empirical correlations of (51) in1979 to study the corrosion rate, subsequently using ribs to study anti-corrosion effects. Despite all this work, there is continued interest in pipe wall corrosion modelling because the prediction of erosion, in particular, is of value in estimating the service life of pipe systems, as well as in the identification of those ocations in a particular pipe geometry most prone to erosion. In this review, computational fluid dynamic model of erosion was developed to investigate the erosion of both the geometries and orientations due to particle collisions with the wall surfaces. Results were discussed in terms of eroded depth and the location of primary and secondary wear, and are compared with available experimental data. This review differs from previous work by the authors (52) which focussed on predicting the characteristics of fluid flow and particle dispersion through duct bends, and from earlier erosion work in considering corrosion in duct rather than mitre bends.

The presence of solid particles enhances the destruction especially 900 mitre bends of protective films giving rise to increased corrosion rates and may add to the overall metal loss by the mechanical erosion of the underlying metal. As with single phase flow these destructive effects are more pronounced under fluid flow condition.

In1991 (46) have developed a predictive model for localized erosion-corrosion under flow pattern conditions based on the application of a two phase flow version of an low Reynolds number (LRN), k-∈ model of turbulence. The motion of the particles was predicted by means of a Lagrangian Stochastic-Deterministic (LSD) model proposed by (53), 1979. The model which was applied to various pipe geometries including a sudden expansion, constriction and a groove was based on an oxygen-mass-transfer controlled corrosion model with the assumption that the particles removed the protective rust film, and an erosion model based on the (54) in2010 cutting wear erosion equations.

In 2009, (55)have successfully applied a two phase k-ε model to the numerical simulation of uniform CO_2 erosion-corrosion under separated flow conditions at a sudden expansion. The particles were modeled by an Eulerian approach.
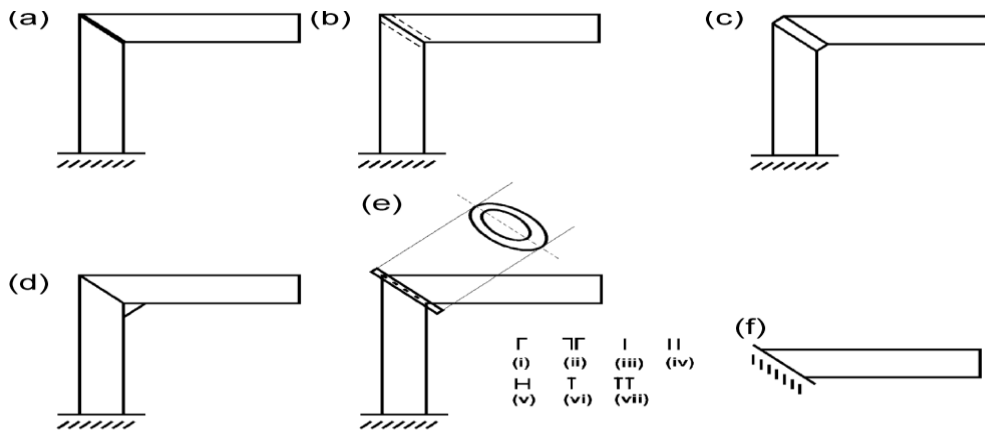
Source: Njobuenwu, D. O., et al (2012)

Fig i: Types of reinforcement in mitred bend
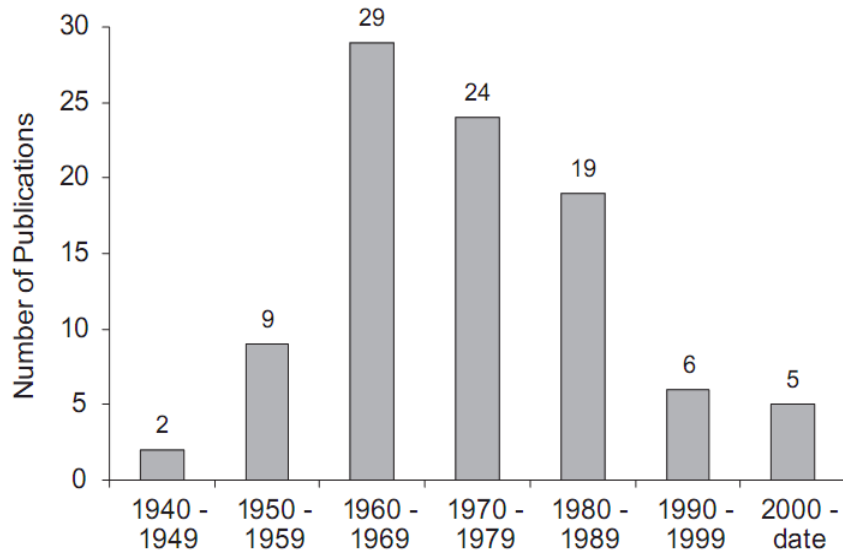
Source: Muhammadu M. M., et al

Fig.ii : Mitre bend publications

The figure ii shown the summaries of the publications that were done in mitre bend represented a form of histogram.

The table below identify any references where corrosion behaviour has been examined. These papers are often experimental in nature.

Table i:
Chronological presentation of single un-reinforced mitred bend detail

Experimental specimen details				Pipe wall thickness- mm
Year (s)	Bend angle (^{0})	Bend radius- mm	Mean pipe radius-mm	Pipe wall thickness- mm
1947	90	195.3	54.1	6.1
1951	90	181.1	130.7	1.4
1951	90	329.6	152.4	3.17
1952	90	175.5	54.1	6.1
1993	90	339.7	152.4	3.17
1952	90	457.1	157.2	8.53
1956	90	457.2	157.2	9.53
1957	90	457.3	81.2	-
1960	90	139.6	-	9.53
1960	90	227.6	1010.4	3.68
1962	90	304.1	76.2	1.23
1963	90	2573.4	156.4	5.0
1964	360	228.6	76.2	3.18
1965	360	228.6	76.2	9.53
1965	360	228.6	76.2	1.22
1966	360	508	156.4	5.0
1968	90	114.3	3.18	48
1970	90	457.7	9.53	16.5
1972	90	1371.6	5.0	31.3
1973	90	914.4	3.12	1.22
1974	90	1143	9.53	16.5
1975	90	1400	924	48.5
1975	90	1219.2	654.1	63.5
1976	90	500	501	9.4
1979	90	1102	226.5	8.2
1981	90	973	499	8.5
1981	360	609.6	150.4	4.1
1983	120	2436.6	25.1	25.4
1985	90	250	9.87	9.87
1988	90	470	4	4
1993	90	1650	21.84	43.68
1995	90	250	124.8	5.9
1995	90	250	126.7	9.87
2007	90	250	124.8	5.9

Source: Muhammadu M.M., et al
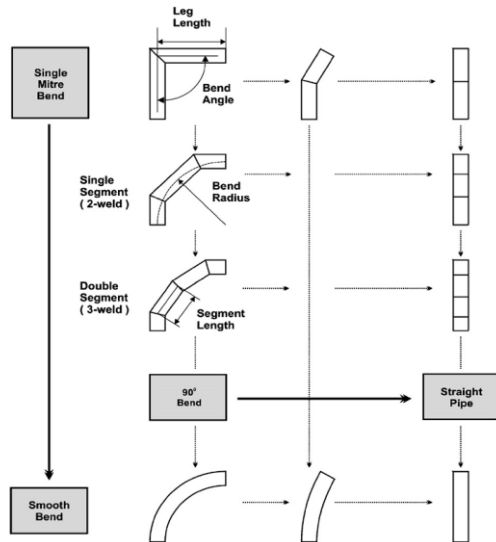
Source: Njobuenwu, D. O., et al (2012)

Fig. iii: Mitred pipe bend 'spectrum'

In Fig. iii, the convergence towards a straight-pipe solution as bend angle increases and towards a smooth pipe solution as the number of segments increases. This means , however, that any welded intersection will give rise to localised corrosion increases, which will in turn be important in relation to wear performance.

Pressure loss / flow characteristics in mitred bends

So far, no attempt has been made in this review to investigate this aspect of mitred bends. To say that this topic has received its fair share of attention in the literature. It is, however, worth highlighting several features of mitre design and analysis which have resulted from these studies. The flow distribution in most mitred bends in a pipeline or ducting system will be non-uniform, due to flow characteristics. This variation has been neglected in most of stress analyses of mitred bends so far undertaken. Commercial computational Fluid dynamics would be extremely useful in the analysis of a bend with some significant variation in pressure/ temperature. Today, fluid–structure interaction software provides the means of predicting such a pressure variation, as well as analysing the structural behaviour of the mitre resulting from the distribution. In this paper, they emphasised the requirement for low-pressure drop. The authors reported that at that time (1960), in a large power station, an expenditure of up to £6000 on each heat exchanger circuit could have been justified for any design feature which would have reduced the circuit pressure drop by 689.5N/m2 (0.1 psi). 3.11. Vibration.

The topics, in relation to mitre bend design fluid vibration, appears to have received little or no attention in the most part World. In contrast to this, the designers of the gas circuits of some French nuclear reactors appear to have given the topic considerable thought in the past. In 1975 (80) investigated the fluid vibration characteristics of the primary gas circuit for the Chinon 3 nuclear reactor. In particular, they investigated the vibration-induced corrosion in the 900 single segment mitred bends which form part of the primary gas circuit in the graphite–gas nuclear reactor. The investigation included the internal guide vanes present to reduce pressure losses. The mitred bends were considered as a source of noise, as a position of noise amplification and finally as an area of special interest in relation to the response of the structure. This paper provides a number of other references (in French), relating to the flow vibration of vaned bend components in the Chinon gas circuit. These references have not been included in this review

III. FLOW ACCELERATED CORROSION

Flow accelerated corrosion (FAC) causes wall thinning (metal thickness loss) of carbon steel piping, tubing and vessels exposed to flowing water or wet steam. When the thickness of the component reaches values lower than the critical thickness required for supporting the operating stresses, it results in ductile failure of the component. If undetected, the degraded components can suddenly rupture, releasing high temperature steam or water. Flow Accelerated Corrosion has resulted in a large number of failures in piping and equipments in all types of fossil, industrial steam, and nuclear power plants and it is a predominant mode of failure of pipelines in the bends and has also affected carbon steel pipelines in the primary circuit of light water (56–63).

The main factor to determine flow accelerated corrosion is the oxide film on structure surfaces, which develops as a results of corrosion and, at the same time, controls the corrosion rate in its role as a protective film (57). The major parameters to determine Flow Accelerated Corrosion are divided into material parameters, flow dynamics parameters and environmental parameters (58). Metallic ions, mainly ferrous ions (Fe^{2+}), are released into the water at the boundary layer where some of the supersaturated Fe2+ ions become oxide particles and they deposit on the metal surface to become a magnetic oxide layer (58). The oxide layer plays an important role in preventing more release of Fe^{2+} (corrosion reaction).

The thickness of the boundary layer is affected by flow dynamics for these processes, oxygen concentration (O_2) in the boundary layer plays an important role for oxidizing magnetite to hematite, which contributes to achieving much higher corrosion resistance (59).

In general, sea pipelines flow assurance covers all multiphase transport phenomena. Diligent design methods, knowledge and skills are needed to ensure safe, continuity of fluids transport from reservoir to topsides processing plant. The main areas involve steady state and transient multiphase flow hydrates, sand, oil, emulsions, wax, scale and corrosion phenomena. The interaction between corrosion/scaling and flow assurance can therefore be of assistance in determining true production rates, and software tools such as the Scand power or radiograghy test or others codes can serve to give reliable predictive modeling. Providing an accurate and reliable link between flow assurance and corrosion modeling is thought to be one of the main challenges facing the industry today. The overriding performance fingerprint is often best recognized as the bath tub curve and to help facilitate this better, corrosion must be considered a functional hazard. Once that is accepted the need for a soundly planned and diligently applied corrosion management strategy becomes self evident and a pronounced requirement for important water sea infrastructure and tie back (60,61,62).

Before now the problems with corrosion integrity during early life is critical, though mid life is often better managed since field life is quite often well below design life and so options and time can be expected to favour planned retrofit if needed. Life extension beyond the wear out zone tends to be more applicable to older researches whereupon original design life's have been exceeded and continued production required (28,31).

3.1 Mechanism of Flow Accelerated Corrosion (FAC)

The mechanism of Flow Accelerated Corrosion is schematically illustrated in Fig. iii. The iron reacts with water to form a surface oxide layer. This oxide dissolves in the water to form Fe2+ and the rate of iron removal (Flow Accelerated Corrosion rate) was controlled by the rate of diffusion of dissolved iron species through the boundary layer of water near the surface into the bulk water. FeOH+ is the hydrolyzed Fe2+ species in solution. This diffusion depends directly on the concentration of soluble iron species at the oxide surface and inversely on the thickness of the boundary layer. Thus, a decrease of the boundary layer thickness because of increased water flow rate or because of local turbulence causes an increase of corrosion rate thus increasing the Flow Accelerated Corrosion rate (1,5–7,63–65). A second effect of flow velocity was related to the solubility limit of the dissolving ionic species in the process water. Process water of a given specific chemistry has a definite solubility limit for ionic species at the given (operating) pH and temperature (65–67). Once the dissolving ions reach the bulk solution (through the boundary layer) and approach the solubility limit, further dissolution is reduced (e.g. in a stagnant solution). This is where the flow acceleration of corrosion rate takes place. The flow velocity provides a fresh solution to the metal surface that has a large capacity to take in the soluble ions thereby increasing the corrosion rate with velocity. Therefore, Flow Accelerated Corrosion is mainly governed by the flow velocity/turbulence affecting the boundary layer on the inside of the pipeline/component and also by the solubility limit of the dissolving ions at the operating parameters.
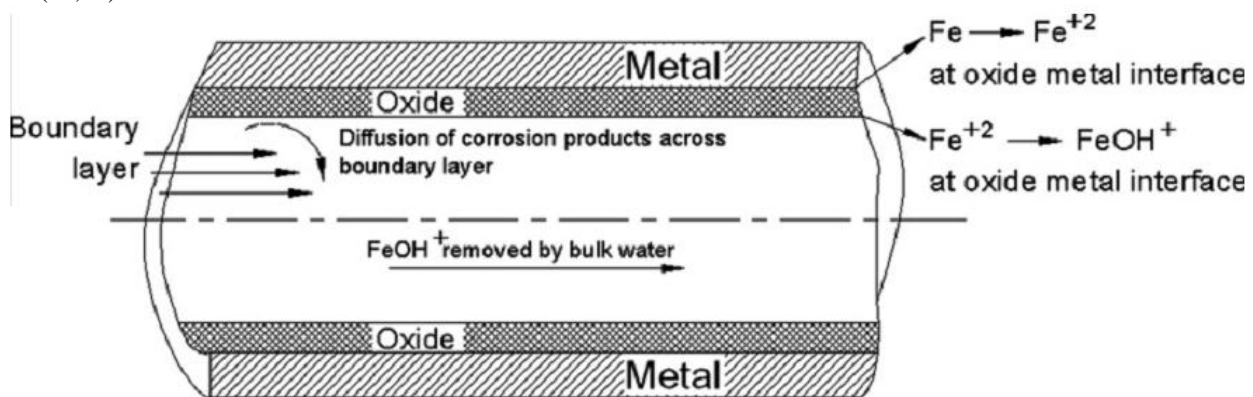
Source: Rybicki, E. F., et al

Fig. iv: Schematic representation of the mechanism of flow accelerated corrosion of steel

.

3.2 Numerical Modelling Approach

The review revealed that there were three (3) main steps are involved in CFD-based erosion-corrosion modelling: flow modelling, particle tracking and erosion-corrosion computation. The development of the Eulerian RANS approach will be used to model the turbulent fluid flow, and of the Lagrangian approach to model the particle trajectories, in a square duct with a 90^0 bend will be describe as a in recent publication (68) in 2012. The validation of both approaches, as well as the computational codes that was used ; hence, these were not be discussed in detail here, (68) in 2012 gave an in depth description of the techniques and methodologies employed.

The mass and momentum conservation equations, expressed in time-averaged form, used in the fluid flow model are given in Equations 2 and 3, respectively:

$$\frac{\partial \bar{u}_j}{\partial x_i} = 0 \qquad (2)$$

$$\bar{u}_j \frac{\partial \bar{u}_j}{\partial x_i} = -\frac{1}{\rho}\frac{\partial \bar{p}}{\partial x_i} + \frac{\partial}{\partial x_i}\left[v\left(\frac{\partial \bar{u}_j}{\partial x_i} + \frac{\partial \bar{u}_j}{\partial x_i}\right) - \overline{u'_\iota u'_J}\right] \quad (3)$$

These equations were closed using the second-moment turbulence closure of Jones and (69) in which the Reynolds stress terms $\overline{u'_\iota u'_J}$ are obtained directly from solutions of modelled partial differential transport equations. Following (70) the closure may be specified as:

$$\frac{\overline{\partial u_\iota u'_J}}{\partial t} + \overline{u_J}\frac{\partial}{\partial x_j}\left(\overline{u'_\iota u'_J}\right) = -\left(\overline{u'_\iota u'_J}\frac{\overline{\partial u_j}}{\partial x_i} + \overline{u'_\iota u'_J}\frac{\overline{\partial u_\iota}}{\partial x_\iota}\right) + C_s\frac{\partial}{\partial x_i}\left[\frac{k}{\epsilon}\overline{u'_\iota u'_m}\frac{\partial}{\partial x_m}\left(u'_\iota u'_J\right)\right]$$

$$+ A_{ij} - \frac{2}{3}\delta_{ij}\varepsilon \qquad (4)$$

Where k is the turbulence kinetic energy and ε its dissipation rate. The redistributive fluctuating pressure term, A_{ij}, is modelled (71; 70) as:

$$A_{ij} = -C_1\frac{\epsilon}{k}\left(\overline{u'_\iota u'_J} - \frac{2}{3}k\delta_{ij}\right) + C_2\delta_{ij}\overline{u'_\iota u'_m}\frac{\overline{\partial u_{\iota J}}}{\partial x_m} + C_3\left(\overline{u'_\iota u'_J}\frac{\overline{\partial u_\iota}}{\partial x_\iota} + \overline{u'_\iota u'_J}\frac{\overline{\partial u_J}}{\partial x_\iota}\right) + C_4 k$$

$$\left(\frac{\partial u_i}{\partial x_j} + \frac{\overline{\partial u_J}}{\partial x_\iota}\right) + C_5\overline{u'_\iota u'_J}\frac{\overline{\partial u_I}}{\partial x_I} - \left(\frac{2}{3}C_2 + C_3\right)\left(\overline{u'_\iota u'_J}\frac{\overline{\partial u_I}}{\partial x_i} + \overline{u'_\iota u'_J}\frac{\overline{\partial u_J}}{\partial x_j}\right)$$

$$- \left(\frac{2}{3}C_4 + C_3\right)k\delta_{ij}\frac{\overline{\partial u_I}}{\partial x_I} \qquad (5)$$

From equation (5) models A_{ij} as a general linear function of the Reynolds stress tensor under the assumption that the "return" and mean strain (or rapid) contributions to the velocity–pressure gradient correlation, normally modelled separately, are directly influenced by the mean strain. The model constants were taken as standard (71), with $C_S = 0.22$, $C_1 = 3.0$, $C_2 = -0.44$, $C_3 = -0.46$, $C_4 = -0.23$, and $C_5 = 0.3$.

The turbulence energy dissipation rate required for solution of equation (4) was obtained (71; 70) from:

$$\frac{\partial \epsilon}{\partial t} + \bar{u}_j \frac{\partial \varepsilon}{\partial x_j} = C_\varepsilon \frac{\partial}{\partial x_l}\left(\frac{k}{\varepsilon}\overline{u'_\iota u'_m}\frac{\partial \varepsilon}{\partial x_m}\right) - C_{\varepsilon 1}\frac{\varepsilon}{k}\overline{u'_\iota u'_m}\frac{\partial \bar{u}_j}{\partial x_m} - C_{\varepsilon 2}\frac{\varepsilon^2}{k} \qquad (6)$$

Where the constants in equation (6) were again taken as standard (71), with $C_\varepsilon = 18$, $C_{\varepsilon 1} = 1.44$, and $C_{\varepsilon 2} = 1.90$.

The particle dynamics were treated in a Lagrangian framework according to the particle equation of motion, $du_p/dt = F/m_p$, where u_p is the particle velocity vector, $m_p = (1/6)\rho_p \pi d^3_p$ is the particle mass and F is the total force acting on the non-rotating, rigid spherical particles in the flow field. In this reviewed the drag, buoyancy, gravity and shear lift forces were included for the dilute gas-particle flows considered since the density ratio of the fluid to the particles was low, $0(10^{-3})$. The particle position vector x_p was again obtained from particle equation of motion, $dx_p/dt = u_p$. The algorithms for F used here have been verified and validated elsewhere, with details given in (68). The effect of the fluid turbulence on the particle motion was accounted for using the random Fourier series method described in (68) and (72) based on the method of (68) and (72). The normal, e_n, and tangential, e_t restitution coefficients describe the action of particles when they collide with a wall. A particle collides with a wall when its centre is one radius from the wall, and it loses a fraction of its momentum before being introduced back into the bulk flow. Assuming particle attrition is negligible, energy at the location of impact will be dissipated as heat, noise and target material deformation. This effect is described by the momentum-based restitution coefficient, e, and the target material deformation was the subject of interest here. The characteristics of e are such that: e = 1 describes an elastic collision, while e < 1 describes an in-elastic collision. The magnitude of e in both directions depends on the particle–wall material pair and the flow system.

In the absence of a particle–wall collision model, then e_n was usually taken as unity. The value of e_t depends on the fluid material. Fluid that bounce off walls have an e_t value close to unity, while fluid that stick to walls would have an e_t value close to zero. In this reviewed, dynamic, empirical restitution coefficients (73) as a function of particle impingement angle, given in equation (7), were considered, as well as wall surface roughness. The inclusion of the wall surface roughness contributes to the re-suspension of fluid after collisions with a wall (74). The wall surface roughness was modelled using a stochastic model (75). Here, the fluid impact angle $\propto = \propto' + \Delta\gamma\varepsilon$ used in equation (7) was assumed to be composed of the fluid trajectory angle to a smooth wall, $\propto'$, and astochastic contribution due to wall roughness, $\Delta\gamma\varepsilon$. ε is a Gaussian random variable with a mean of zero and a standard deviation of unity, with a roughness angle of 3.8^0 used in the present work (75).

$$e_n = 1.0 - 0.4159\propto + 0.4994\propto^2 - 0.292\propto^3$$

$$e_t = 1.0 - 2.12\propto + 3.0775\propto^2 - 1.1\propto^3 \qquad (7)$$

From five different erosion model. The erosion ratio (also known as the erosion ate), ER, is defined here as the ratio of the eroded mass of the target material to the mass of impinging particles. The erosion with due to consideration of the ability of each model to predict the ductile The solid particle erosion model is in the general form, $E = Kf(\propto)u^n_p$, with the erosion-corrosion rate given as $ER = E/m_p$ and the eroded depth as $ED = (ER_{lc} \times m_p)/(\rho w \times A_{cell})$. The units used in this reviewed for E, ER and ED were mg, mg g^{-1} and mm, respectively. Here, u_p was the fluid impact velocity, $f(\propto)$ is a dimensionless function of the impact angle, K is generally taken as a constant depending on the properties of the target material, abrasive material, shape and other factors, n is a velocity exponent, m_p is the mass of the particle, ρ_w is the density of the wall material, and A_{cell} is the area of the computational cell where the impingement occurs. ER_{lc} is the local erosion ratio computed material erosion-corrosion characteristic of having maximum erosion at an acute particle impingement angle.

3.4 Flow Accelerated Corrosion in primary circuit of a nuclear power plant

The primary circuit of Pressurized Heavy Water Reactors contains heavy water with pH (at 25^0C) adjusted in the range of 9.5–10.5, by addition of lithium hydroxide, to minimize corrosion and keep the corrosion products in soluble form.

Hydrogen addition is also done to suppress radiolytic oxygen production and the temperature in the primary circuit is in the range of 250–297^{0}C in 220 MWe PHWRs. Magnetite solubility (or indirectly the Flow Accelerated Corrosion rate) is dependant upon the temperature and the pH (15–17). Solubility of magnetite which is directly proportional to the Flow Accelerated Corrosion rate, reduces with increase in temperature below a pH of 9.8. Above a pH of 9.8 the solubility of magnetite increases with temperature (15–17) resulting in higher dissolution of magnetite. There is an inversion in the temperature dependence of solubility at the pH range of 9.8–10.3. High pH is beneficial in retarding Flow Accelerated Corrosion rate at lower temperatures but at higher temperatures, pH higher than 9.8 results in greater dissolution of the magnetite itself. In the primary circuit of the nuclear power plants the pH and temperature combination results in greater dissolution of magnetite causing a higher Flow Accelerated Corrosion rate

IV. DEGRADATION AT BEND

The review revealed that the bend feed water system from the secondary side in a reactor was replaced as thinning had been measured. The extrados region of the bend had thinned down considerably as shown in Fig. iv. The internal surface of the bend was seen to be very rough and there was considerable loss of wall thickness at the extrados. At one point the wall thickness had reduced to 0.71 mm. This region of extensive thinning is marked in Fig. 3. The thickness measured at the intrados was 6.46 mm. Thinning of the bend had also extended into the straight section of the pipe to some extent as shown in Fig. 6a. Fig. 6b shows the other section of the pipe away from the bend where thinning was not appreciable.

The bend was cut open and the internal surface was observed using a stereo microscope. Fig. iv shows the surface pattern seen at different regions of the internal surface marked 'A' to 'E'. Different features were observed at different regions of the bend. Region marked 'A'' shows formation of grooves. The regions marked 'B' showed some 'scallop' like features indicating occurrence of some single phase flow accelerated corrosion. The thinning observed in this region was not extensive indicating that extent of degradation due to Flow Accelerated Corrosion was not appreciable. The regions marked 'C' was near to the extensive thinning region. Steps had formed and the surface was very rough indicating extensive localized removal of material. The region marked 'D' is at the extrados. In this region also steps can be seen and extensive localized thinning was observed. At the intrados region (region marked 'E') there was no clear feature formed.

Degradation and thinning has occurred to a lesser extent at the intrados. There were no clear features on the internal surface indicating the occurrence of single/dual phase Flow Accelerated Corrosion. However, in the regions of extensive localized thinning/grooving the direction of the grooves were in the flow direction. These regions of extensive thinning (region 'C') had also extended into the straight section of the pipe to an initial distance of about 25 mm downstream of extrados. Thinning was not observed in other regions of the pipe section. Formation of signature patterns characteristic of single phase or dual phase flow accelerated corrosion were not observed in this region. The reduction in thickness in the extrados is thus attributed to 'flow rate '.

4.1 Metallurgical analysis of the bend turbine stage 2 drain

The review revealed that the following samples were examined for establishing the mode of degradation: (1) Pipe piece from extraction-6 drain line and (2) bend that was being used at turbine stage II drain of HP turbine. It was in operating condition in the secondary system until thickness measurement obtained with the help of ultrasonic testing in the plant showed that it had got degraded in thickness and its residual life was lowered. The operating parameters were: (1) Temperature: around 2000C, (2)operating pressure: 40 kg/cm2 and (3) water chemistry: (a) Deoxygenated water and (4) pH: 8.8–9.5 maintained with the help of ETA. The chemical analysis and the optical micrographs of the materials showed it to be a low carbon steel. XRD analysis on the ID side of the samples showed the presence of magnetite as well as that of haematite. The samples examined are shown in Fig. v.
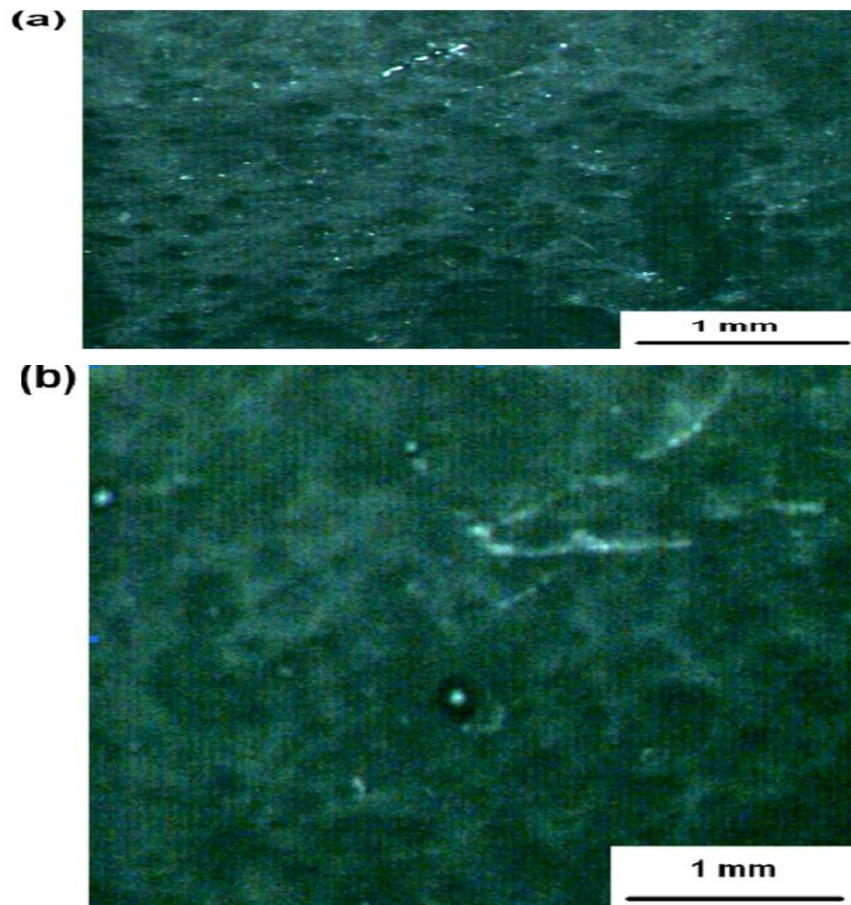
Source: Rybicki, E. F., et al
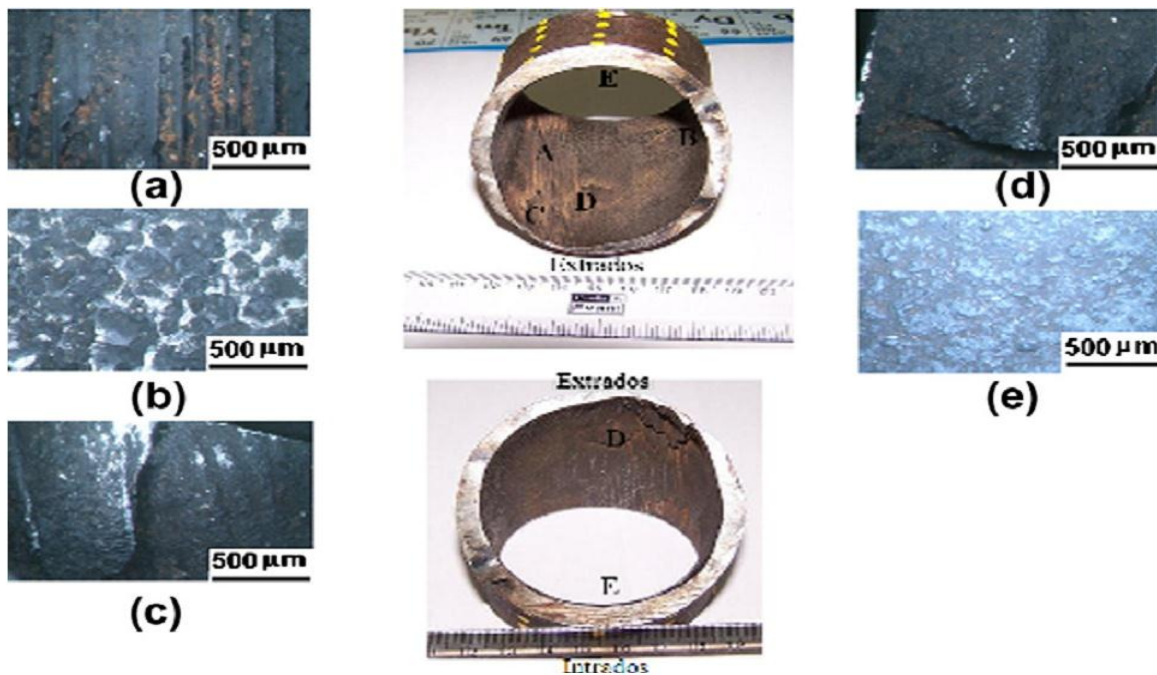
Fig.v: Surface features observed on the internal surface of the bend at different regions Marked 'A' to 'E'.
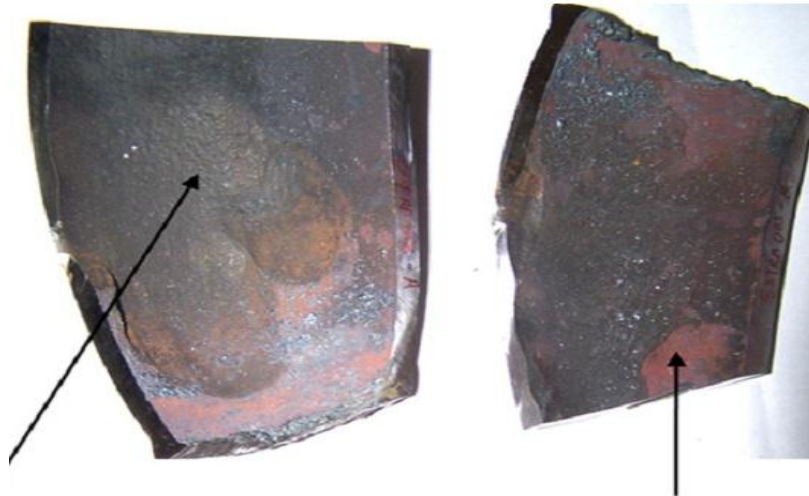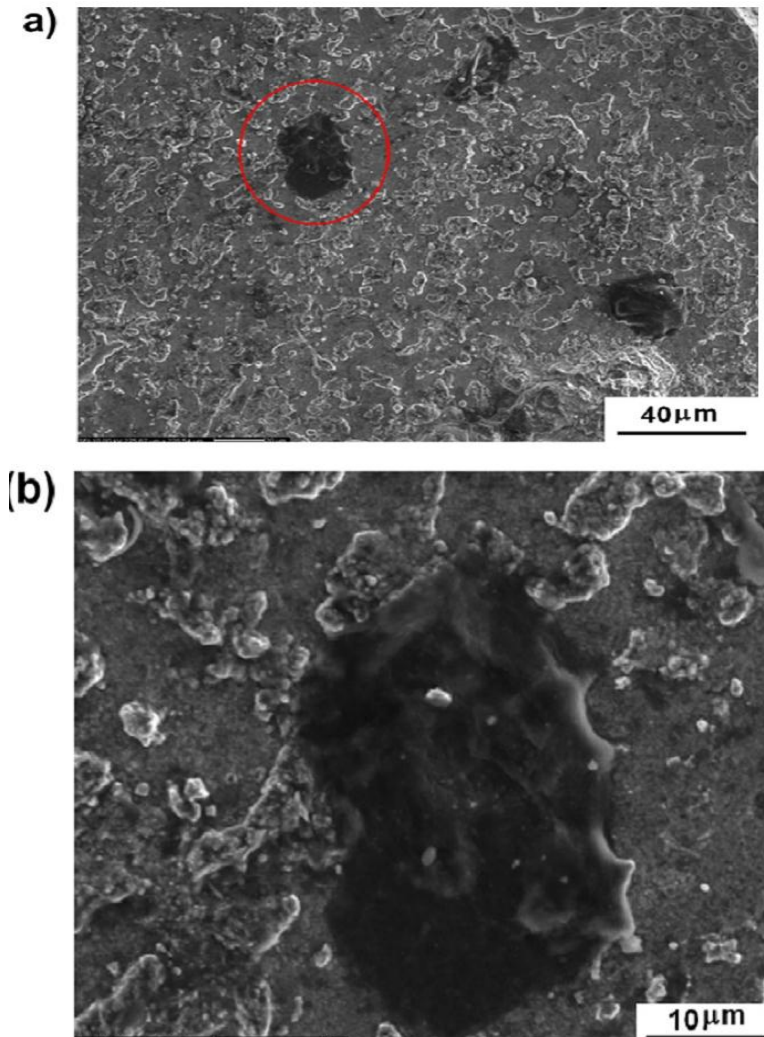
Source: Rybicki, E. F., et al

Fig.vi: cut sample of extrados of the extraction drain line from the region with maximum thinning.

Source:Rybicki,E.F.,eael

Fig. vii: Stereomicroscopic images of thinned pipe sample.

Source: Rybicki, E. F., et al

Fig. viii: SEM images (a) and (b) showing absence of specific surface patterns and indications   erosion-corrosion damage.

4.2 Stereo microscopy

This revealed that stereomicroscopy was done so as to examine the surface morphology at a higher magnification. However, due to highly black layer of oxide the surface features were not clear (Fig. vii) and even extra source of light was not able to reveal the features. Flow Accelerated Corrosion was generally associated with characteristic horse shoe pit structure with orange peel appearance, and dual phase Flow Accelerated Corrosion was associated with tiger striping. From the images (Fig. vii no specific pattern could be observed.

4.3 Scanning electron microscopy

Scanning electron microscopy of the sample which usualllly taken from the region of maximum thinning was done to reveal surface morphology so as to see if there are any sign of Flow Accelerated Corrosion (scallops). Signature appearance of Flow Accelerated Corrosion was absent indicating there cannot be Flow Accelerated Corrosion. Also on going into higher magnification, review revealed that there are some signs of erosion-corrosion (Fig.7). On examination of the images at higher magnification it was indicated that some material has been removed by impact of fluid (of few microns).

It was inferred that this particular case was not directly attributable to Flow Accelerated Corrosion as no distinct signature of Flow Accelerated Corrosion was observed on the affected surfaces. The observations indicate erosion-corrosion taking place in the system that is clear from SEM examination of the affected surfaces that show impingement/erosion features (Fig. 7). These features are not observed/reported from Flow Accelerated Corrosion affected components (76,77,78,79).

V. CONCLUSION

A comprehensive review of literature available on aspect of mitred bend behaviour reveals that there is no experimental solution available which is applicable to the complete range of bends found in industry.

A computational fluid dynamic model coupled to a Lagrangian particle tracking routine and a number of erosion-corrosion models have been used to predict the solid particle erosion-corrosion in mitre bends for dilute particle-laden flow. A number of Flow Accelerated Corrosion related degradations have occurred in both the primary and the secondary circuit of nuclear power plants. However, thinning was largely attributed to fabrication and Flow Accelerated Corrosion.

This paper also describes the mechanism of Flow Accelerated Corrosion. It has been illustratively shown that each case of thinning degradation, at least once at a given location in the plant, needs to be analysed to establish the exact cause of degradation.

REFERENCES

[1] Cubicciotti D. Flow assisted corrosion of steel and the influence of Cr and Cu additions. J NuclMater 1988;151:255–64.

[2] Villien B, et al. In: Proceedings of the twenty sixth annual CNS-CNA student conference, Toronto; June 2001.

[3] Smith CL, Shah VN, Kao T, Apostolakis G. NUREG/CR-5632: incorporating aging effects into probabilistic risk assessment – a feasibility study utilizing reliability physics models. US Nuclear Regulatory Commission; 2001.

[4] Dooley RB, Chexal VK. Flow-accelerated corrosion of pressure vessels in fossil plants. Int J Pres Ves Pip 2000;77:85–90.

[5] Ho Moon J, et al. Dependency of single phase FAC of carbon steel and low alloy steels for NPP system piping on pH, orifice distance and material. Nuclear Eng Technol 2005;37:371–82.

[6] Shoji T, Lu Z, et al. Towards proactive materials degradation management in NPP – today and future. In: CD proceedings of the 14th Asia Pacific corrosion control conference (APCCC), October 21–24, 2006, Shanghai, China; 2006.

[7] International Atomic Energy Agency. Material degradation and related managerial issues at nuclear power plants. In: Proceedings of technical meeting held during February 15–18, 2005 at Vienna by International Atomic Energy Agency (IAEA); 2006.

[8] Hales C, et al. Boiler feedwater pipe failure by flow assisted chelant corrosion. Eng Fail Anal 2002;9:231–33.

[9] ASM Handbook. Corrosion – fundamentals, testing and protection, vol. 13A. ASM International, The Materials Information Society, Materials Park, Ohio; 2003.

[10] Kain V, Prasad GE, Gadiyar HS. Erosion corrosion of carbon steel components in contact with ammoniacal solutions. Industral J Technol 1992; 30:341–6.

[11] Wood, R. J. K.,et al (2001). Upstream swirl induction for reduction of erosion damage from slurries in pipeline bends. Wear, 250(1–12), 765–772.

[12] Meng, H. C., and Ludema, K. C. (1995). Wear models and predictive equations – Their form and content. Wear, 181–183(2), 443–457.

[13] Finnie, I. (1960). Erosion of surfaces by solid particles. Wear, 3(2), 87–103.

[14] Bitter, J. G. A. (1963a). A study of erosion phenomena: Part I. Wear, 6(1), 5–21.

[15] Bitter, J. G. A. (1963b). A study of erosion phenomena: Part II. Wear, 6(3), 166–185.

[16] Hashish, M. (1987, 7–10 September). An improved model of erosion by solid particle impact. Paper presented at the 7th international conference on erosion by liquid and solid impact, Cambridge, UK.

[17] Wallace, M. S., Dempster, W. M., Scanlon, T., Peters, J., & McCulloch, S. (2004). Prediction of impact erosion in valve geometries. Wear, 256(9–10), 927–936.

[18] Suzuki, M., Inaba, K., & Yamamoto, M. (2008). Numerical simulation of sand erosion in a square-section 90-degree bend. Journal of Fluid Science and Technology, 3(7), 868–880.

[19] Yakhot, V., et al, (1986). Renormalization group analysis of turbulence. Basic theory. Journal of Scientific Computing, 1(1), 3–51.

[20] Forder, A., Thew, M., & Harrison, D. (1998). A numerical investigation of solid particle erosion experienced within oilfield control valves. Wear, 216(2), 184–193.

[21] Neilson, J. H., & Gilchrist, A. (1968). Erosion by a stream of solid particles. Wear, 11(2) 111–122.

[22] Wallace, M. S. (2001). CFD-based erosion modelling of simple and complex geometries (Ph.D. thesis). University of Strathclyde, Strathclyde.

[23] Habib, M. A., et al (2007). Erosion rate correlations of a pipe protruded in an abrupt pipe contraction. International Journal of Impact Engineering, 34(8), 1351–1368.

[24] Badr, H. M., et al, (2005). Numerical investigation of erosion threshold velocity in a pipe with sudden contraction. Computers & Fluids, 34(6), 721–742.

[25] Habib, M. A., et al (2007). Erosion rate correlations of a pipe protruded in an abrupt pipe contraction. International Journal of Impact Engineering, 34(8), 1350–1369.

[26] Badr, H. M., et al (2004). Numerical calculations of erosion in an abrupt pipe contraction of different contraction ratios. International Journal for Numerical Methods in Fluids, 46(1), 19–35.

[27] Habib, M. A., et al (2008). Erosion and penetration rates of a pipe protruded in a sudden contraction. Computers & Fluids, 37(2), 140–150.

[28] Ben-Mansour, R., et al (2006). Erosion in the tube entrance region of an air-cooled heat exchanger. International Journal of Impact Engineering, 32(9), 1441–1460.

[29] Al-Anizi, S. S., et al, (2006). Solid-particle erosion in the tube end of the tube sheet of a shell-and-tube heat exchanger. International Journal for Numerical Methods in Fluids, 50(8), 881–890.

[30] Ahlert, K. R. (1994). Effects of particle impingement angle and surface wetting on solid particle erosion of AISI 1018 steel. Tulsa, OK: The University of Tulsa.

[31] Shirazi, S. A., et al (2001). Modeling solid particle erosion in elbows and plugged tees. Journal of Energy Resources Technology, 123(4), 277–284.

[32] McLaury, B. S. (1996). Predicting solid particle erosion resulting from turbulent fluctuations in oilfield geometries (Ph.D. thesis). The University of Tulsa, Tulsa, OK.

[33] Shirazi, S. A., McLaury, B. S., Shadley, J. R., & Rybicki, E. F. (1995). Generalization of theAPI RP14E guideline for erosive services. Journal of Petroleum Technology, 47(8),693–698.

[34] Rybicki, E., et al (1996). Application of flow modeling and particle tracking to predict sand erosion rates in elbows. ASME Fluids Engineering Division, 236, 725–734.

[35] Rybicki, E. F., et al (1995). Generalization of the API RP14E guideline for erosive services. Journal of Petroleum Technology, 47(8),693–698.

[36] Forder, A. (2000). A computational fluid dynamics investigation into the particulate erosion of oilfield control valves (Ph.D. thesis). University of Southampton, Southampton, UK.

[37] Thew, M., and Harrison, D. (1998). A numerical investigation of solid particle erosion experienced within oilfield control valves. Wear, 216(2), 1804–190.

[38] Bourgoyne, A. T. (1989). Experimental study of erosion in diverter systems due to sand production. Paper presented at the SPE/IADC drilling conference, SPE/IADC 18716, New Orleans, LA.

[39] Chen, X. H., et al, (2004). Application and experimental validation of a computational fluid dynamics (CFD)-based erosion prediction model in elbows and plugged tees. Computers & Fluids, 33(10), 1251–1272.

[40] Shirazi, S. A., et al (2006a). A comprehensive procedure to estimate erosion in elbows for gas/liquid/sand multiphase flow. Journal of Energy Resources Technology, 128(1), 71–75.

[41] Shirazi, S. A.,et al, (2006b). Numerical and experimental investigation of the relative erosion severity between plugged tees and elbows in dilute gas/solid two-phase flow. Wear, 261(7–8), 715–729.

[42] Tabakoff, W., Kotwal, R., & Hamed, A. (1979). Erosion study of different materials affected by coal ash particles. Wear, 52(1), 161–173.

[43] Wang, J. R., & Shirazi, S. A. (2003). A CFD based correlation for erosion factor for long-radius elbows and bends. Journal of Energy Resources Technology, 125(1), 26–34.

[44] Kim, W. J., et al (1994). Origin and decay of longitudinal vortices in developing flow in a curved rectangular duct. Journal of Fluids Engineering, 116(1) 45–52.

[45] Eyler, R. (1987). Design and analysis of a pneumatic flow loop (M.Sc. thesis). West Virginia University, Morgantown, WV.

[46] Nesic, S., & Postlethwaite, J. (1991). A predictive model for localized erosion corrosion. Corrosion, 47(8), 582–589.

[47] Nesic, S., et al (2000). Particle tracking and erosion prediction in three-dimensional bends. In 2000 ASME fluids engineering division summer meeting, FEDSM2000-11249 Boston, MA.

[48] Bergevin, K. (1984). Effect of slurry velocity on the mechanical and electro-chemical components of erosion–corrosion in vertical pipes (M.Sc. thesis). University of Saskatchewan, Saskatoon, Canada.

[49] Hanson, R., & Patel, M. K. (2000). Development of a model to predict the life of pneumatic conveyor bends subject to erosive wear. In ASME fluids engineering division summer meeting, FEDSM2000-11246 Boston, MA.

[50] Meng, T., et al (2009). Numerical simulation of predicting and reducing solid particle erosion of solid–liquid two-phase flow in a choke. Petroleum Science, 6(1), 95–97.

[51] Njobuenwu, D. O. (2010). Modelling and simulation of particulate flows in curved ducts (Ph.D. thesis). University of Leeds, Leeds, United Kingdom.

[52] Menguturk, M., and Sverdrup, E. F. (1979). Calculated tolerance of a large electric utility gas turbine to erosion damage by coal gas ash particles. In W. F. Adler (Ed.), Erosion: prevention and useful applications (pp. 193–224). Philadelphia: American Society for Testing and Materials, ASTM-STP-664.

[53] Finnie, I. (1960). Erosion of surfaces by solid particles. Wear, 3(2), 87–103.

[54] Rybicki, E. F., et al (2010). A two-dimensional mechanistic model for sand erosion prediction including particle impact characteristics. In NACE international annual conference, corrosion 2010 (Paper No. 10377) San Antonio, TX.

[55] Shirazi, S. A., et al (2009). Improvements of particle near-wall velocity and erosion predictions using a commercial CFD code. Journal of Fluids Engineering, 131(3), 031303–031309.

[56] Cubicciotti D. Flow assisted corrosion of steel and the influence of Cr and Cu additions. J Nucl Mater 1988;152:259–64.

[57] Villien B, Zheng Y, Lister DH. In: Proceedings of the twenty sixth annual CNS-CNA student conference, Toronto; June 2001.

[58] Smith CL, et al, NUREG/CR-5632: incorporating aging effects into probabilistic risk assessment – a feasibility study utilizing reliability physics models. US Nuclear Regulatory Commission; 2001.

[59] Chexal VK., et al Flow-accelerated corrosion of pressure vessels in fossil plants. Int J Pres Ves Pip 2000;77:81–89.

[60] Kim Uh Ch, et alDependency of single phase FAC of carbon steel and low alloy steels for NPP system piping on pH, orifice distance and material. Nucl Eng Technol 2005;37:375–84.

[61] Shoji T, Lu Z, Takeda Y, Sato Y. Towards proactive materials degradation management in NPP today and future. In: CD proceedings of the 14th Asia Pacific corrosion control conference (APCCC), October 21–24, 2006, Shanghai, China; 2006.

[62] International Atomic Energy Agency. Material degradation and related managerial issues at nuclear power plants. In: Proceedings of technical meeting held during February 15–18, 2005 at Vienna by International Atomic Energy Agency (IAEA); 2006.

[63] Owens AD et al, Boiler feed water pipe failure by flow assisted chelant corrosion. Eng Fail Anal 2002;9:235–43.

[64] Remy F N, et al, Flow-assisted corrosion: a method to avoid damage. Nucl Eng Des 1992;133:23–30.

[65] Kain V, et al, Flow accelerated corrosion and control strategies in the secondary circuit pipelines in Indian nuclear power plants. J Nucl Mater 2008;383:86–91.

[66] Watanabe Y., et al Effects of Cr content and environmental factors on FAC rate of carbon steels. In: Proceedings of 2009 ASME pressure vessel and piping division conference, July 26–30, 2009, Prague, Czech Republic (CD-ROM), PVP2009-78126.

[67] Ziemniak SC, Jones ME, Combs KES. Magnetite solubility and phase stability in alkaline media at elevated temperatures. J Sol Chem 1995;24:837–77.

[68] Njobuenwu, D. O., et al (2012). Prediction of turbulent gas–solid flow in a duct with a 90◦ bend using an Eulerian–Lagrangian approach. AIChE Journal, 58(1), 14–30.

[69] Oka, Y. I., Okamura, K., and Yoshida, T. (2005). Practical estimation of erosion damage caused by solid particle impact. Part 1: Effects of impact parameters on a predictive equation. Wear, 259(1–6), 95–101.

[70] Jones, W. P.,et al (1988). Closure of the Reynolds stress and scalar flux equations. Physics of Fluids, 31(12), 3589–3604.

[71] Dianat, M., et al, (1996). Reynolds stress closure applied to axisymmetric, impinging turbulent jets. Theoretical and Computational Fluid Dynamics, 8(6), 435–447.

[72] Fan, J. R., et al, (1997). New stochastic particle dispersion modeling of a turbulent particle-laden round jet. Chemical Engineering Journal, 66(3), 207–215.

[73] Jun, Y. D., et al (1994). Numerical-simulation of a dilute particulate flow (laminar) over tube banks. Journal of Fluids Engineering, 116(4), 770–777.

[74] Tsuji, Y., and Morikawa, Y. (1982). LDV measurements of an air–solid two-phase flow in a horizontal pipe. Journal of Fluid Mechanics, 120, 382–405.

[75] Sommerfeld, M., et al, (1999). Experimental analysis and modelling of particle wall collisions. International Journal of Multiphase Flow, 25(6–7),1457–1489.

[76] International Atomic Energy Agency. Material degradation and related managerial issues at nuclear power plants. In: Proceedings of technical meeting held during February 15–18, 2005 at Vienna by International Atomic Energy Agency (IAEA); 2006.

[77] Kain V, et al, Erosion corrosion of carbon steel components in contact with ammoniacal solutions. Ind J Technol 1992;30:341–6.

[78] Kain V, et al, Flow accelerated corrosion and control strategies in the secondary circuit pipelines in Indian nuclear power plants. J Nuclear Mater 2008;383:86–91.

[79] Kain V., et al. (2011) Flow Accelerated Corrosion: Experience from examination of components from nuclear power plant, pp 2025-2032.

[80] Baylac G, Copin A. Vibration studies of the new primary circuit of the chinon 3 reactor. In: Transactions of the third international conference on structural mechanics. In reaction technology paper F4/3, London, 1–5 September 1975.